Matched template analysis of continuous wave laser for space debris ranging application

Available online at www.sciencedirect.com

ScienceDirect

Advances in Space Research xx (2022) xxx-xxx

ADVANCES IN SPACE RESEARCH (a COSPAR publication)

www.elsevier.com/locate/asr

Matched Template Analysis of Continuous Wave Laser for Space Debris Ranging Application

Shasidran Raj[a,b,*], Samuel Francis[a,b], Lyle Roberts[a,b], Robert Ward[a], David McClelland[a], Daniel Shaddock[a]

[a] *Centre for Gravitational Physics, Department of Quantum Science, The Australian National University, Building 38a, Science Road, ACT, 2601, Australia*
[b] *Space Environmental Research Centre, Mount Stromlo Observatory, Stromlo, ACT, 2611, Australia*

Received 1 May 2013; Received in final form 10 May 2013; Accepted 13 May 2013;
Available online 15 May 2013

Abstract

The growth of human-made space debris, sharing the same Earth's orbital space as active satellites, is a worrying environmental condition. Precise tracking and orbital modelling of space debris are vital to predict potential future collisions with active satellites. This paper investigates a continuous-wave laser ranging method where a bench-top experiment models the reflected amplitude modulated optical signal from a space debris target. The optical signal is digitised and stored to undergo post-digital signal processing using a parameter estimation matched filter approach to estimate the time-varying delay between the target debris and the observing telescope. The experiment investigated two different detection methods, the direct detection of the optical signal and the coherent detection where the optical signal is amplified with a bright local oscillator before signal detection. The experimental results show that the coherent detection method can provide a more precise time-varying delay estimate than the direct detection method due to the improved signal-to-noise ratio. The experimental results also show improved precision in the parameter estimation when using larger portions of the acquired signal's time series. The experimental results were used to model for a potential space debris application. For example, assuming the received signal power from the target debris is approximately 3.5 fW, the time-varying delay of the target debris using the coherent detection method can be estimated with a precision of 1 m/s using 2.5 s of the acquired signal time series. This is well within the expected minimum time series that can be collected from a space debris target from a single flyover at the telescope site.

Keywords: Space Debris Ranging; Continuous Wave Laser; Match Filter Analysis; Parameter Estimation; Pseudo-Random Noise Code

1. Introduction

Since the 1960s, human-made space debris in Earth's orbit has been increasing at an alarming exponential rate (SDp, 2019). The increased congestion in the limited available space in Earth's orbit increases the likelihood of a collision between the different orbiting objects. Each collision and fragmentation event could cause significant damage to active satellites (Shoots, 2009) and accelerates the number of orbiting space debris, leading to a runaway chain reaction called the Kessler Syndrome (Kessler & Cour-Palais, 1978). In 2019, the European Space Agency (ESA) has stated that 11.6 non-deliberate fragmentation events occur each year (Agency, 2019) and this number is expected to increase in the future.

The Space Environmental Research Centre (SERC) is investigating using a high powered continuous-wave laser with aim of manoeuvring space debris for collision avoidance in highly congested regions of Low Earth Orbit (LEO) (Mason et al., 2011) and improving current ranging methods to better estimate the orbital motion of target debris. The proposed bench-top experiment is required to be compatible with the research into the ground-based continuous-wave laser manoeuvring system (Roberts, 2016) and models a space debris application. The

*Corresponding author

https://dx.doi.org/10.1016/j.jasr.xxxx.xx.xxx
0273-1177/

outgoing continuous-wave laser is amplitude modulated with a pseudo-random noise (PRN) code. The target debris has a complex orbital motion with a time-varying delay, where the propagation distance changes with time, between the target and the observing telescope. The reflected beam from the space debris target is collected by the telescope and the digitised optical signal is saved for post-digital signal processing. The digitised optical signal undergoes a matched filter analysis approach to estimate the time-varying delay of the space debris and used to predict potential future collisions and determine the impact of the de-orbiting attempt on the debris' orbit.

2. Space Debris Laser Ranging Concept

Most current space debris ranging systems, including the EOS telescope used by SERC (Greene, 2016), use a pulsed laser source to measure the propagation delay of each transmitted pulse between the telescope and target debris. The change in propagation delay for each pulse can be used to determine the time-varying delay. Equation 1 can be used to estimate the received signal power P_{Sig} from the target, depending on the transmitted optical power P_T, laser wavelength λ, active collecting area of the telescope A_T, target range R, reflecting area of the target debris A_{SD}, atmospheric loss F^2 and loss for non-cooperative space debris targets β.

$$P_{Sig} = P_T \frac{(A_T A_{SD})^2}{(R\lambda)^4} F^2 \beta \tag{1}$$

One of the main challenges with precisely tracking space debris is the lower signal power reflected from the target debris compared to an active satellite. SERC are interested in tracking space debris between 1 cm and 10 cm, resulting in a small A_{SD} value, hence low P_{Sig} in Equation 1. Space debris is also considered a non-cooperative target. An active satellite has an onboard retro-reflector (Lehr, 1966; Kirchner et al., 2012; UNT, 1999) to maximise the reflection of the optical signal parallel to the incident beam. Small pieces of space debris would not have a retro-reflector and may have an unstable orbit. Therefore the optical signal is scattered, resulting in a small signal power reflected towards the telescope, and may fluctuate. The parameter β in Equation 1 is used to take into account signal loss due to the scattered reflection of a space debris target. Both β and F parameter values are difficult to model and could vary depending on the daily condition, the target's surface and the telescope system. If either parameter is equal to 1, there is no signal loss. SERC also plans on using adaptive optics (Bennet et al., 2015) to reduce atmospheric effects on the propagating beam.

Figure 1 also shows a space debris target has a complex reflective surface, hence increasing the signal loss β from scattering and also introducing a random phase effect (Overbeck, 1994). The reflected electric field from the diffuse surface would have a varying random propagating distance due to the rough surface with varying depth of x m. The random propagation distance results in each reflected electric field having a random phase (Paschotta, 2008b). The electric fields interfere with each other to produce a speckle pattern and reduce the summed electric field of the optical signal. Therefore a phase modulation approach used in a coherent detection method for delay measurements (Francis et al., 2014; Sutton et al., 2010) cannot be used for the low signal-to-noise ratio application for space debris ranging. Hence, this paper investigates using an amplitude modulation approach where the randomised phase of the reflected signal would not impact the range measurement.

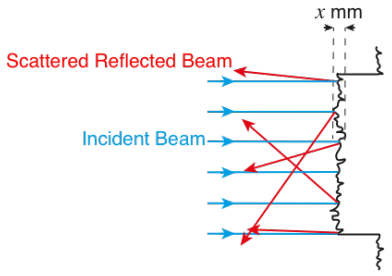

Fig. 1: Illustration of the scattering effect of the incident optical signal from a diffuse surface.

Table 1 shows some of the fixed parameter values used as input to Equation 1 based on the EOS telescope facility and SERC's design for the ground-based laser system. The proposed 10 kW continuous-wave laser would be amplitude modulated with a PRN code to avoid complications from the diffuse reflecting surface of the space debris. The reflected signal is collected by the telescope where the acquired optical signal is digitised and stored for post-digital signal processing at a later time. Section 3 will discuss the analysis approach to estimate the time-varying delay of the acquired optical signal. Section 4 will discuss the bench-top experiment modelling the reflected signal from a space debris target and the two different detection methods. Section 5 presents the analysis results of the digitised optical signals from the bench-top experiment and Section 6 will discuss the results for possible space debris application.

Table 1: **Parameters values used as input to equation 1 to calculate P_{Sig}.**

Parameter	Chosen Parameter Values
Transmitted Power P_T	10 kW
Laser wavelength λ	1064 nm
Telescope Aperture	1.8 m
Space debris diameter	1 cm to 10 cm
Minimum LEO Range R	500 km

3. Estimating Target Position with Time-Varying Delay

The outgoing optical signal is amplitude modulated with a PRN code. A PRN code is a deterministic binary sequence where the sequence output has random properties but the entire sequence is periodic (Mutagi, 1996). PRN codes sequences are used in various position measurement applications, such as Gold codes in GPS and path length measurements of optical signals (Francis et al., 2014; Roberts, 2016). Amplitude modulated PRN codes are also used in atmospheric and satellite ranging applications (Matthey & Mitev, 2004; Norman & Gardner, 1988).

The target space debris has complex orbital motion, which from the reference point of the observing telescope has a time-varying delay $\tau(t)$, where the initial propagating distance d_0 between the telescope and target changes over time with varying velocity v_0, acceleration a_0 and other higher derivatives of motion. Equation 2 shows the time-varying propagation delay $\tau(t)$ of the optical signal reflected by a moving space debris target.

$$\tau(t) \simeq \frac{1}{c}\Big(d_0 + v_0 t + \frac{a_0 t^2}{2}\Big) \tag{2}$$

A matched filter is a signal processing tool used to look for the presence of the desired signal by cross-correlating the measured time series with a template signal (Turin, 1960). The time-varying delay of the target space debris causes a Doppler shift of the modulated PRN code frequencies, which no longer matches the original template code. Therefore a parameter estimation approach where different values for each parameter are used to alter and attempt to match the template code to the acquired signal. This approach allows the analysis to estimate the time-varying delay parameter values such as d_0 and v_0 of the target debris. This form of parameter estimation is used in many digital signal processing applications to identify weak and unknown signals obscured by noise in the time series, such as matched filtering analysis of optical signals acquired by LIGO observatories to determine the properties of the detected gravitational waves (Owen & Sathyaprakash, 1998; Gabbard et al., 2018).

Figure 2 shows an illustration of using the parameter estimation matched filter analysis with PRN codes. In a space debris application, the time-varying delay parameters of the target are not known, therefore the matched filter analysis generates a range of possible values for each parameter of interest. In Figure 2, only the distance d_0 and velocity v_0 parameters are used to alter the template code. If the d_0 is increased, the template code is shifted in time. If v_0 increases, the change in time-varying delay causes the template code to appear more stretched. The template code is aligned to match the acquired signal only when the parameter value for distance d_0 and velocity v_0 are equal to the time-varying delay of the target.

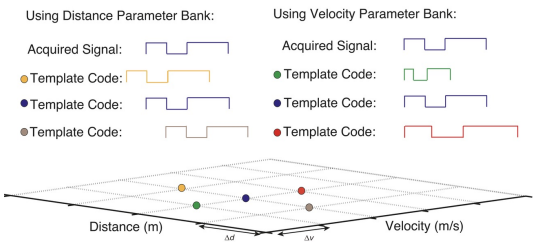

Fig. 2: Simulated matched filter analysis where only the input value for the distance parameter is changed.

Figure 3 shows the correlation output between the acquired signal with the template code for d_0 and v_0 parameter values. The most significant correlation output is produced when the acquired signal is aligned to the template PRN code, indicating the parameter values are matched. Therefore the signal correlation can be used to determine the space debris' d_0 and v_0 parameter values. If parameters such as acceleration and jerk are required, or other parameter than impact the orbital properties, additional input parameters can be added to the analysis. In a space debris application, some orbital information of the target debris would be known and can be used to determine the impact of each parameter in Equation 2 as well as reduce the size of the template bank for each parameter.

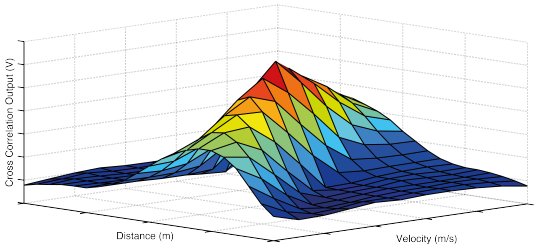

Fig. 3: Cross-correlation output between the acquired signal and template code for varying input parameter values.

4. Optical Bench-Top Experimental Layout

The optical bench-top experiment presented in this section aims to model the received signal power from a space debris target where the amplitude-modulated PRN code is Doppler shifted due to the time-varying delay. The experimental setup can be broken up into the following steps:

1. Generate a Doppler shifted PRN code sequence
2. Amplitude modulate the continuous wave laser
3. Attenuate the optical signal before the signal acquisition
4. Signal acquisition with either the direct or coherent detection scheme
5. Estimate the time-varying delay of the modulated PRN code

Figure 4 shows the optical layout of the bench-top experiment used for both detection schemes. The laser source in the bench-top experiment is a free-running 1064 nm wavelength laser, without phase-locking or frequency stabilisation of the laser source, and maximum output intensity of approximately 200 mW. The output of the laser source is split into two using a beam splitter. The first output is used as the input to a Fibre Mach-Zehnder interferometer to amplitude modulate the laser beam and used as the signal beam. The second output is used as the local oscillator to interfere with the signal beam in the coherent detection scheme. In the direct detection scheme, the local oscillator beam is blocked.

4.1. Fibre Mach-Zehnder Interferometer

The input optical power of the Fibre Mach-Zehnder interferometer is split equally into two arms using a 1×2 fibre splitter. Equation 3 shows the electric field of the two arms of the Fibre Mach-Zehnder interferometer. The first path is called the *phase modulation arm* represented by the electric field $E_{Mod}(t)$ where a Photline EOM (Photline, 2017) is used to phase modulate the laser with the Doppler-shifted PRN code (ϕ_{PRN}). The second

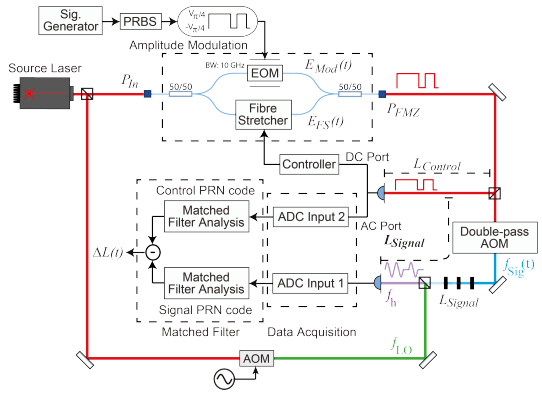

Fig. 4: The bench-top experimental setup used for the direct and coherent detection schemes.

path is called the *fibre stretcher arm* containing a fibre stretcher with the electric field $E_{FS}(t)$. The fibre stretcher is used to control the optical path length, and hence the phase ϕ_{FS} of the fibre stretcher arm.

$$E_{Mod}(t) = E_{Mod}e^{i(2\pi f_{Laser}t+\phi_{Mod}+\phi_{PRN})}$$
$$E_{FS}(t) = E_{FS}e^{i(2\pi f_{Laser}t+\phi_{FS}(t))} \quad (3)$$

The PRN code is generated using a Keysight N4970A Pseudo-Random Bit Stream (PRBS) generator (PRB, 2012). The frequency of the output PRN code can be changed between 50 MHz and 12.5 GHz using a signal generator. In the bench-top experiment, the unshifted PRN code chip frequency chosen is 75 MHz. Assuming the target debris is moving at 7 km/s, using the Doppler shift equation for change in frequency ($\delta f = \frac{v_{SD}}{c} f_{chip}$), the PRN code chip frequency is Doppler shifted by 1750 Hz. A 15-bit PRN code is chosen for the bench-top experiment with a code repetition rate of 0.4 ms at 75 MHz and the ambiguity range is 130 km. The short PRN code length is chosen to reduce complexity in the signal analysis stage as the bench-top experiment path length is less than 130 km. The PRBS generator can produce longer PRN code with an ambiguity range as high as 33 000 km which is suitable for LEO space debris applications. The Doppler-shifted PRN code generated by the PRBS generator (75 MHz $\pm \delta f$) is phase modulated using the EOM in the Fibre Mach-Zehnder interferometer.

The two arms of the Fibre Mach-Zehnder interferometer are recombined using a 2x1 fibre coupler. The two electric fields interfere with each other, and the output optical signal of the Fibre Mach-Zehnder P_{FMZ} is shown in equation 4. The resulting interference pattern depends on the phase difference $\phi_{\Delta L}$ of the two arms (Hariharan, 1992), which is equal to $\phi_{Mod} - \phi_{FS}$, and the PRN code phase modulation ϕ_{PRN}.

$$P_{FMZ}(t) = \frac{P_{In}}{2} + \frac{P_{In}}{2}\cos(\phi_{\Delta L} + \phi_{PRN}(t)) \quad (4)$$

Figure 5 and Equation 5 shows the change in the output optical power P_{FMZ} due to the PRN code modulation. The desired phase difference $\phi_{\Delta L}$ is achieved by controlling the input voltage to the optical fibre stretcher in the fibre stretcher arm to change L_{FS} so that $\phi_{\Delta L}$ is equal to $\frac{3\pi}{2}$. The fibre stretcher also reduces fluctuations in $\phi_{\Delta L}$ due to temperature fluctuations or vibrations and independent path length changes of the two arms of the Fibre Mach-Zehnder interferometer (Muller et al., 2006).

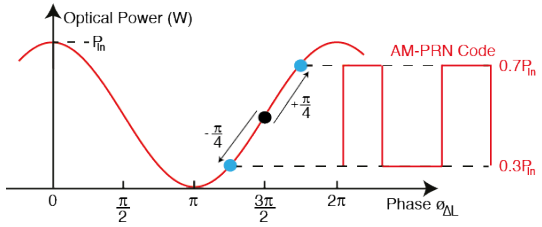

Fig. 5: Illustration of the interference of two laser beams as a function of the difference in the phase of the two laser beams. The phase difference $\phi_{\Delta L}$ is equal to $\frac{3\pi}{2}$ and a $\pm\frac{\pi}{4}$ phase modulation is added using ϕ_{PRN}.

$$P_{FMZ}(t) = \begin{cases} \frac{P_{In}}{2} + \frac{P_{In}}{2}\cos\left(\frac{3\pi}{2} + \phi_{PRN}\right) \approx 0.7P_{In}, & \text{if } \phi_{PRN} = \frac{\pi}{4} \\ \frac{P_{In}}{2} + \frac{P_{In}}{2}\cos\left(\frac{3\pi}{2} - \phi_{PRN}\right) \approx 0.3P_{In}, & \text{if } \phi_{PRN} = -\frac{\pi}{4} \end{cases} \quad (5)$$

Figure 5 shows a $\frac{\pi}{2}$ ($\pm\frac{\pi}{4}$) phase modulation was chosen for the PRN code since between $\frac{7\pi}{4}$ and $\frac{5\pi}{4}$ the output optical power is approximately linear. The result is an amplitude modulated optical signal ranging between $0.7P_{In}$ and $0.3P_{In}$. In the ideal case, a π modulation depth would be applied to have a full intensity modulation of the laser between P_{In} and 0. However, the current control layout, could not apply the full intensity modulation due to the combination of fluctuations in the PRN code from the PRBS and $\phi_{\Delta L}$. A future iteration of the bench-top experiment will investigate using a full-modulation depth but since the bench-top experiment was investigating low optical power operation, this lower modulation depth produced a lower intensity output optical signal.

4.2. Measuring Different Propagating Path Lengths

In Figure 4, the output of the Fibre Mach-Zehnder interferometer is then split into two separate paths:

1. *Control path* - used to measure and control the optical intensity fluctuations for the Fibre Mach-Zehnder interferometer and to measure $L_{Control}$ path length
2. *Signal path* - used to attenuate the optical signal and measure L_{Signal} path length

The PRN code generated by the PRBS is free running and cannot be synchronised with the start of the data acquisition. This means each time the PRN code is collected from both the control and the signal path has a random but the same L_{Code} path length. To remove the influence of the L_{Code} path length in the measurements, the path length difference between the control and the signal path is used in the analysis. On the bench-top experiment the physical path length measured for L_{Signal} is equal to 2.75 m and for $L_{Control}$ is equal to 0.675 m. Therefore the physical path length difference ΔL is 2.075 m.

4.3. Comparing the Different Detection Methods

In Figure 4 the signal path is passed through a *Double-pass AOM* optical configuration to frequency shift the laser frequency $f_{Sig}(t)$ by 160 MHz using a Acousto-Optic Modulator (AOM) (Paschotta, 2008a). The output of the Double-pass AOM is then attenuated using several *Neutral Density* (ND) filters to achieve the desired optical signal power before signal detection and acquisition.

The main difference between the *direct detection scheme* and *coherent detection scheme* is the use of the local oscillator. In the direct detection scheme, the local oscillator path is blocked and the attenuated optical signal is directly measured using the photodetector. A Newport 1811 free-space photodetectors (NF1, 2001) is used in both the signal and control path. The minimum noise equivalent power (NEP) of the photodetector is 22.5 pW/$\sqrt{\text{Hz}}$ between 10 MHz and 200 MHz (NF1, 2001) and is the dominant noise in the direct detection scheme.

In the coherent detection scheme, the local oscillator is first frequency-shifted by 90 MHz using an AOM (Paschotta, 2008a). The local oscillator is used to interfere and amplify the attenuated signal beam before detection at the photodetector. The resulting interference pattern will have a heterodyne beat note of 70 MHz. The output power of the local oscillator is 110 μW, allowing the amplification of the optical signal until shot noise from the local oscillator is the dominant noise source above the photodetector noise. Any further increase in the local oscillator optical power would not amplify the optical signal as shot noise also increases, resulting in the same signal-to-noise ratio.

Coherent detection methods are sensitive to frequency fluctuations. The bench-top experiment aims to test the coherent detection scheme by introducing a random frequency noise and $\frac{1}{f}$ frequency noise from a second free-running laser source. These additional steps were taken to test the impact on the matched filter analysis steps if additional frequency noise is introduced into the signal path laser from signal propagation, loss of frequency stabilisation and frequency drift.

The double-pass AOM is also used to introduce additional frequency noise into the optical signal by adding a random noise source to the carrier frequency of the AOM ($f_{Sig}(t) \pm \delta f_{Noise}(t) = 160\,\text{MHz} \pm 5\,\text{MHz}$). A second experimental layout is also carried out as shown in Figure 6 where the local oscillator beam is replaced with a second fibre coupled laser source. The second laser source is also free-running, without frequency stabilisation and phase-locking where the resulting heterodyne beat note is allowed to drift over time.

4.4. Signal Detection and Signal Analysis

As previously discussed, the attenuated optical signal for both detection schemes is acquired using a Newport 1811 photodetector. The photodetector splits the measured optical intensity into two frequency bandwidths. The DC port produces signals between DC and 50 kHz. This port is used to measure small fluctuations from the control path as an error signal feedback to the fibre stretcher. The AC port produces signals between 25 kHz and 125 MHz containing the 75 MHz chip frequency amplitude-modulated PRN code.

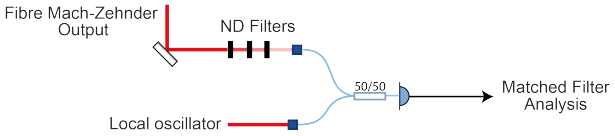

(a) Signal laser is interfered in fibre with the local oscillator from the same laser source.

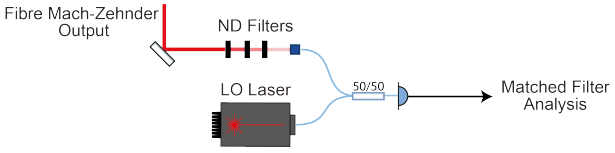

(b) Signal laser is interfered in fibre with the local oscillator from a second laser source.

Fig. 6: Optical layout illustrating the bench-top experiment used to investigate the impact of $\frac{1}{f}$ laser frequency noise on the time-varying delay measurement.

The optical signals measured at both the signal and control path photodetectors are digitised using a NI-5771 analogue to digital converter (ADC) (NI5, 2012). The ADC has a sampling frequency of 1.5 GHz. The digitised signal is then saved onto a desktop computer to perform post-digital signal processing with the matched filter analysis discussed in Section 3. The ADC also adds a propagation delay of approximately 0.33 ns between the signal and control path. This results in extra 0.1 m added to the path length difference where ΔL is expected to equal 2.175 m. Due to the limitations of the on-board memory during the digitisation stage, the maximum length of the acquired signal's time series for the analysis is limited to 0.1 s.

For the coherent detection scheme, the digitised optical signal is first passed through an I&Q demodulation stage as shown in Figure 7 before the matched filter analysis. I&Q demodulation is used to extract the amplitude-modulated PRN code from the heterodyne beat note.

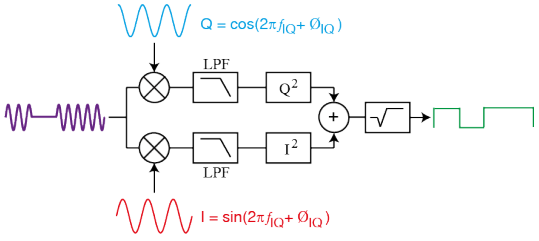

Fig. 7: Block diagram of the I&Q demodulation steps to recover the amplitude modulated PRN code from heterodyne beat note.

Equation 6 shows the output amplitude of the I&Q demodulation A_{IQ} depends on the recovered PRN code $C(t - \tau_{Sig})$, optical signal power P_{Sig} and local oscillator power P_{LO}. The recovered PRN code $C(t - \tau_{Sig})$ is amplified by the local oscillator power P_{LO} but remains unaffected by the laser frequency or phase noise from the signal or local oscillator beams.

$$\begin{aligned} A_{IQ} &= 2\sqrt{Q^2 + I^2} \\ &= 2C\Big(t - \frac{L_{Sig}}{c}\Big)\sqrt{P_{LO}P_{Sig}} \end{aligned} \tag{6}$$

4.5. Summary of Bench-top Experiment

Table 2: **Table summarising the parameters chosen for the optical bench-top experiment.**

Parameter	Parameter Values
ADC sampling frequency $f_{sampling}$	1.5 GHz
PRN chip frequency f_{chip}	75 MHz
PRN code length L	15-bit ($2^{15}-1$)
Max. Collected Time Series (Max t_i)	0.1 s
Laser wavelength λ	1064 nm
Photodetector NEP	22.5 pW/$\sqrt{\text{Hz}}$
Photodetector bandwidth f_{PD}	125 MHz
Signal freq shift f_{Sig} (changeable)	160 MHz
LO freq shift f_{LO}	90 MHz
LO Optical Power P_{LO}	110 μW
Heterodyne beat note f_h (changeable)	70 MHz

5. Experimental Results

The experimental results from the two detection scheme are passed through the same matched filter analysis for comparison.

5.1. Signal Correlation for Doppler Shifted PRN code

Figure 8 shows the signal correlation generated by the matched filter analysis using the coherent detection scheme where P_{Sig} is equal to 20 nW and the acquired signal length t_i used by the analysis is 1 ms from the maximum 0.1 s of the collected data. The modulating PRN code is Doppler shifted to model a target travelling at −7000 m/s (75 MHz + 1750 Hz). The most significant position of the signal correlation is used to estimate d_0 and v_0 parameters. Together with using the matched filter analysis result for the control path, the measured path length difference ΔL ($L_{Signal} - L_{Control}$) is equal to 2.21 m and v_0 is equal to −7016 m/s. For the same P_{Sig}, t_i and matched filter analysis steps, the direct detection scheme estimated ΔL equal to 2.52 m and v_0 is equal to −6527 m/s.

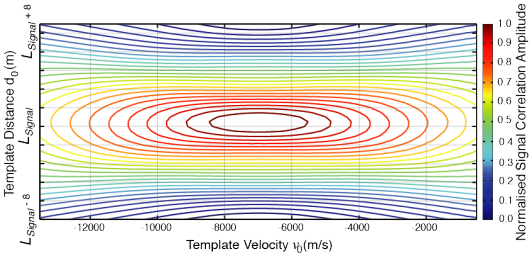

Fig. 8: Contour plot showing the signal correlation produced by the matched filter analysis for the coherent detection scheme.

5.2. Precision for Varying Received Signal Power P_{Sig}

Figure 9 shows the precision in matched filter analysis estimate of the time-varying delay for different P_{Sig}, comparing both the direct and coherent detection scheme. The mean precision for the time-varying delay estimate was obtained using 25 different acquired signals from the bench-top experiment for each P_{Sig}. The analysis is repeated for 3 different integration times t_i.

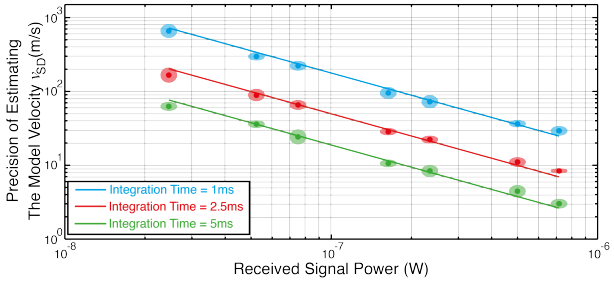

(a) Precision for the direct detection scheme. Each fitted line has a slope of −1.

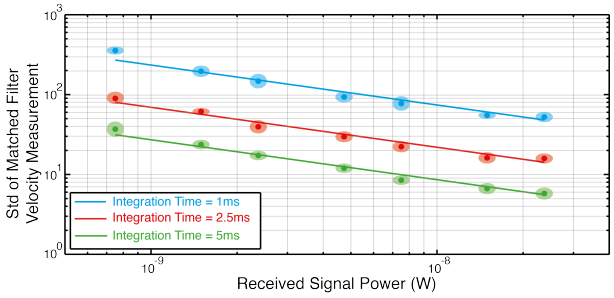

(b) Precision for the coherent detection scheme. Each fitted has a slope of −0.5.

Fig. 9: Precision of estimating v_{SD} as a function of P_{Sig} for both the direct detection and coherent detection scheme.

For the direct detection scheme results in Figure 9a, the slope of the signal correlation changes linearly with P_{Sig}. Therefore a line fitted to the mean precision of the matched filter analysis with a slope of −1 in logarithmic scale for each analysis time t_i. For the coherent detection scheme results in Figure 9b, the slope of the signal correlation changes by 2 $\sqrt{P_{Sig}P_{LO}}$. As P_{LO} is fixed during the signal acquisition, precision is expected to change by $\sqrt{P_{Sig}}$. Therefore a line fitted to the mean precision of the matched filter analysis with a slope of −0.5 in logarithmic scale for each analysis time t_i. In both methods, the result matches the expected change in the precision for varying P_{Sig}.

5.3. Precision for Varying Analysis Time t_i

Figure 10 shows the relationship between precision and t_i for both the direct and coherent detection schemes. Unlike the impact of P_{Sig}, the change in t_i is expected to be the same for both detection schemes. When increasing t_i, the slope of the signal correlation increases by t_i^2. Increasing the integration time linearly increases the peak of the signal correlation but also linearly reduces the Full-Width Half Maximum (FWHM) of the signal correlation. Both make the slope of the signal correlation steeper. However, increasing t_i also increases the noise in the signal correlation by $\sqrt{t_i}$. Therefore the expected relationship between precision in estimating the velocity parameter and t_i is $t_i^{1.5}$. Figure 10a and Figure 10b show that for the direct and coherent detection scheme respectively with a line fitted to the mean precision of the matched filter analysis with a slope of −1.5 in logarithmic scale for each P_{Sig}. The result matches the expected change in the precision for varying t_i.

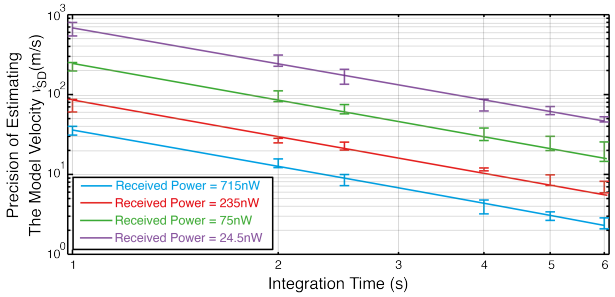

(a) Precision of estimating v_{SD} for direct detection scheme.

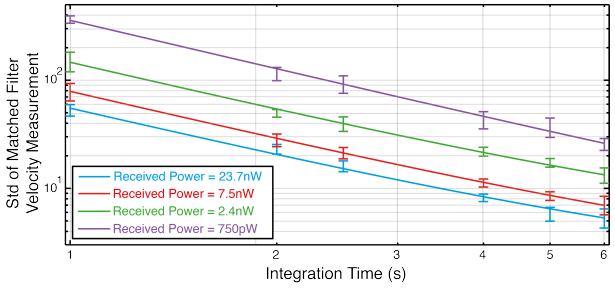

(b) Precision of estimating v_{SD} for coherent detection scheme.

Fig. 10: Precision of estimating v_{SD} for varying integration times. For both schemes, each trend line has a relationship of $t_i^{-1.5}$.

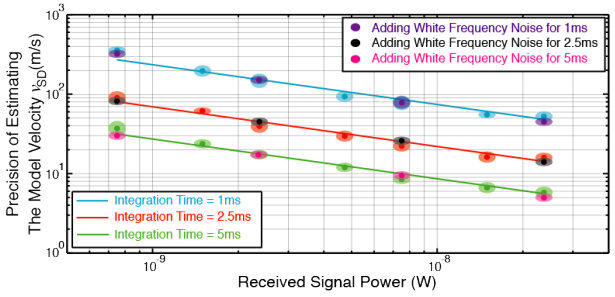

(a) Adding Random Frequency Noise to experimental setup.

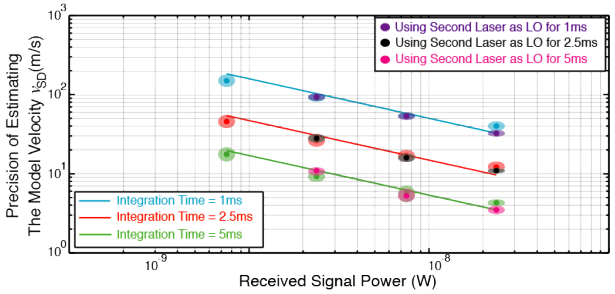

(b) Adding $\frac{1}{f}$ laser frequency noise from second local oscillator source

Fig. 11: Comparing the matched filter analysis results for the coherent detection scheme when adding both random and free-running laser frequency noise.

5.4. Adding Laser Frequency Noise to Signal Path

Coherent detection methods are sensitive to changes in both the frequency and phase of the optical signal. In most applications, the laser sources are frequency stabilised (Black, 2001) or derived from the same source to maintain a stable phase. Section 2 discussed the challenges in using a phase modulation method due to the random phase effect. This led to the development of the direct detection method where the amplitude-modulated PRN code is not affected by the phase and frequency. However, using a coherent method where the local oscillator is used to amplify the signal can improve the precision of analysis parameter estimation.

Section 4.4, presented an altered version of the bench-top experiment to compare the analysis results when using a local oscillator from the same laser source to using a second laser source. A random frequency noise ($\delta f_{Noise}(t) = \pm 5$ MHz) was added using the Double-pass AOM in the signal path. Since the signal acquired from the coherent detection scheme is passed through an IQ demodulation stage prior to the signal analysis stage, only the amplitude information is present, as shown in Section 4.4. Both the phase and frequency information, including the introduced noise, is removed. The results of introducing the two frequency noise sources are presented in Figure 11.

When comparing the results in Figure 11, both results match the expected results without the addition of the two frequency noise sources. This shows that the IQ demodulation has successfully removed the frequency noise added to the signal path and heterodyne beat note in the coherent detection scheme.

6. Discussion on Experimental Results

Using the experimental results in Figure 9 and Figure 10, Equation 7 and Equation 8 are generated to calculate the precision in estimating the time-varying delay for the direct and coherent detection scheme respectively.

$$\sigma_{v_{DD}}\ m/s = 224.35\,\mathrm{m/s}\Big(\frac{75\,\mathrm{nW}}{P_{Sig}\ W}\Big)\Big(\frac{1\,\mathrm{ms}}{t_i\ s}\Big)^{1.5} \tag{7}$$

$$\sigma_{v_{CD}}\ m/s = 150.59\,\mathrm{m/s}\Big(\sqrt{\frac{2.4\,\mathrm{nW}}{P_{Sig}\ W}}\Big)\Big(\frac{1\,\mathrm{ms}}{t_i\ s}\Big)^{1.5} \tag{8}$$

P_{Sig} and t_i are variable parameters in both Equation 7 and Equation 8. As discussed in Section 2, it is difficult to predict the P_{Sig} of a non-cooperative space debris target, as the signal power is dependent on many factors. However, t_i can be changed during the analysis to achieve the desired precision in estimating the time-varying delay parameters. From Table 1, due to the slew rate, the lowest altitude space debris the EOS telescope can track is 500 km. For simplicity of the following discussions, P_{Sig} from the target debris is assumed to be 3.5 fW and the EOS telescope can acquire and store a maximum of 500 s of the optical signal's intensity, taking into account time loss due to orbit profile and target acquisition by the telescope.

To achieve a 1 m/s precision, the coherent detection method would approximately require an analysis time t_i of 2.5 s of the 500 s acquired signal data but this is not possible for the direct detection scheme as it requires 47.5 minutes. Assuming for debris manoeuvring application, a 1 mm/s precision is required, the coherent detection scheme would need 250 s of the 500 s acquired signal data. The direct detection method would need 83 hours.

The coherent detection scheme is more suitable for space debris applications than the direct detection scheme. The coherent detection scheme can achieve the desired 1 m/s precision using acquired signal data collected from a single flyover by amplifying the optical signal with the local oscillator to improve the signal-to-noise ratio. If P_{Sig} is lower than 3.5 fW, t_i can be increased using the acquired signal data. Since the local oscillator noise is the dominant noise source, the coherent detection scheme is less susceptible to variations in background photon noise, allowing space debris ranging operation during daylight hours, currently not possible by many space debris ranging systems (UNT, 1999), and produce more consistent results in a day-to-day application. Even though the different laser sources would be phased locked and frequency stabilised, the results in Section 5.4 show that the coherent detection scheme can still perform the signal analysis if frequency or phase noise and frequency drift are introduced during the laser beam's propagation through the atmosphere and target reflection.

Despite the results, the direct detection scheme could still be used in a space debris application. The EOS telescope uses an avalanche photo-diode (APD) which has a much lower noise floor than the Newport 1811 photodetector used in the bench-top experiment. With the improved signal-to-noise ratio, the direct detection scheme can perform better than the results present in this paper. However, this depends on the NEP of the chosen APD and background photon noise, which may fluctuate from day-to-day resulting in varying precision. Another consideration is the analysis has only assumed a single flyover by the space debris target. Using multiple flyovers could also improve the overall precision of both detection methods.

7. Conclusion

This paper investigated a bench-top experiment with two detection methods to model the optical signal reflected from a target space debris. The acquired signal from the bench-top experiment is stored and passed through a matched filter analysis with parameter estimation to estimate the time-varying delay introduced in the reflected optical signal.

The experimental results and following discussions show that the coherent detection scheme is able to produce a more precise estimate of the time-varying delay due to the amplification of the optical signal before the signal acquisition, hence improving the signal-to-noise ratio. The experimental results also show the coherent detection scheme is not affected by additional frequency noise and drift that could be introduced during signal propagation and reflection and due to the amplification stage is less susceptible to background photon noise. This could allow daylight operation for space debris ranging with more consistent results for day-to-day operations.

8. Acknowledgments

This research was conducted by the Australian Research Council Centre of Excellence for Gravitational Wave Discovery (OzGrav) through project number CE170100004. The research was also supported under a student scholarship from the Space Environment Research Centre.

References

(1999). *Technical Report on Space debris*. Technical Report United Nations Publications.

(2001). *125-MHz Photoreceivers Models 1801 and 1811*. New Focus.

(2012). *Agilent N4970A PRBS Generator 10Gb/s User Guide*. Technical Report Agilent Technologies.

(2012). *NI 5771R User Guide and Specifications*. National Instrument.

(2019). *Orbital Debris Quarterly News*. Technical Report 1 2 NASA Orbital Debris Program Office.

Agency, E. S. (2019). *ESA's Annual Space Environmental Report*. Technical Report ESA Space Debris Office.

Bennet, F., eline D'Orgeville, C., Gaob, Y., Gardhousea, W., Paulina, N., Pricea, I., Rigauta, F., Ritchieb, I., Smithb, C., Uhlendorfa, K., & Wangb, Y. (2015). Adaptive optics for space debris tracking. In *Adaptive Optics Systems IV*. Proc. of SPIE volume 9148.

Black, E. (2001). An introduction to pound–drever–hall laser frequency stabilization. *Am. J. Phys.*, *69*, 70 – 87.

Francis, S. P., Lam, T. T.-Y., McKenzie, K., Sutton, A. J., Ward, R. L., McClelland, D. E., & Shaddock, D. A. (2014). Weak-light phase tracking with a low cycle slip rate. *Optics Letters*, *39*, 5251–5254.

Gabbard, H., Williams, M., Hayes, F., & Messenger, C. (2018). Matching matched filtering with deep networks for gravitational-wave astronomy. *Phys. Rev. Lett.*, *120*(141103).

Greene, B. (2016). Optical techniques for space environment management. In *Advance Maui Optical and Space Surveillance*. Maui, Hawai'i: Space Environment Research Centre.

Hariharan, P. (1992). *Basics of Interferometry*. (1st ed.). Academic Press.

Kessler, D. J., & Cour-Palais, B. G. (1978). Collision frequency of artificial satellites: Creation of a debris belt. *Journal of Geophysical research*, *83*(A6), 2637 – 2646.

Kirchner, G., Koidl, F., Friederich, F., Buske, I., Volker, U., & Riede, W. (2012). Laser measurements to space debris from graz slr station. *Advances in Space Research*, *51*, 21–24.

Lehr, C. G. (1966). Satellite tracking with a laser. *SAO Special Report*, (215).

Mason, J., Stupl, J., Marshall, W., & Levit, C. (2011). Orbital debris-debris collision avoidance. *Pergamon*, *48*(10), 1643–1655.

Matthey, R., & Mitev, V. (2004). Pseudo-random noise-continuous-wave laser radar for surface and cloud measurements. *Optics and Lasers in Engineering*, *43*(3–5), 557 – 571.

Muller, H., Peters, A., & Braxmaier, C. (2006). Optical fibers with interferometric path length stability by controlled heating for transmission of optical signals and as components in frequency standards. *Applied Physics*, *84*, 401 – 408.

Mutagi, R. (1996). Pseudo noise sequences for engineers. *Electronics Communication Engineering Journal*, *8*(2), 79–87.

Norman, D. M., & Gardner, C. S. (1988). Satellite laser ranging using pseudonoise code modulated laser diodes. *Applied Optics*, *27*(17).

Overbeck, J. A. (1994). *Comparison of Coherent to Incoherent Detection at 2.09 um using a Solid State LADAR System*. Technical Report Wright Laboratory.

Owen, B. J., & Sathyaprakash, B. S. (1998). Matched filtering of gravitational waves from inspiraling compact binaries: Computational cost and template placement. *Physical Review D*, *60*(2).

Paschotta, R. (2008a). *acousto-optic modulators*. Encyclopedia of Laser Physics and Technology. URL: `https://www.rp-photonics.com/acousto_optic_modulators.html`.

Paschotta, R. (2008b). *Optical Phase*. ISBN 978-3-527-40828-3. Wiley-VCH.

Photline (2017). *NIR-MPX-LN series 1000nm band Phase Modulators*. Phase Modulators iXblue 3, Rue Sophie Germain France.

Roberts, L. (2016). *Internally Sensed Optical Phased Arrays*. Phd thesis The Australian National University.

Shoots, D. (2009). Orbital debris quartely news.

Sutton, A., McKenzie, K., Ware, B., & Shaddock, D. (2010). Laser ranging and communications for lisa. *Optical Express*, *18*(20).

Turin, G. I. (1960). A introduction to matched filters. *IEEE Transactions on Information Theory*, *6*(3), 311 – 329.